OPTIMAL DESIGN OF COMPOSITE INSERTS FOR A HYBRID ULTRACENTRIFUGE ROTOR

Hak Gu Lee[1*], Jisang Park[1], Ji Hoon Kim[1]
[1] Composite Materials Group, KIMS, Changwon, Korea
* Corresponding author(hakgulee@kims.re.kr)

Keywords: *centrifuge, hybrid composite rotor, composite insert, optimization*

1 Introduction

An ultracentrifuge is essential equipment in bioindustry to separate tiny biogenic substances such as hormones. The equipment should be able to generate the *G*-force (gravitational force) higher than 600,000 × *g*. Among diverse components of an ultracentrifuge, a fixed angle type rotor is the most important component that affects the equipment's performance.

There have been several studies related to rotating structures. The problem on the stress distribution of a rotating isotropic disc with a central hole is a well-known example[1]. A rotating anisotropic disc was firstly analyzed by Tang, and he derived the analytic solutions of the centrifugal stresses[2]. Belingardi also considered a rotating anisotropic disc, but constructed approximated solutions[3].

Studies concentrated on designing centrifuge rotors are as follows. Hai-jun carried out failure analysis of an isotropic centrifuge rotor, and suggested how to optimize the rotor structure[4]. Joe designed a hybrid type composite rotor, in which carbon fiber/epoxy composites were wound around a polymeric core[5]. Among diverse design studies, Joe's design is one of the most feasible rotors that can be manufactured with low cost.

A hybrid composite rotor having a polymeric core experiences stress concentration phenomenon near tube holes that accept sample fluids to be separated. The stress concentration of the core can be alleviated by bonding composite inserts into the tube holes. In this study, the dimensions of the composite inserts are optimized in order to reduce the stress concentration. Using a simplified slice disc model, which give us a more conservative design than a 3-D rotor model does, stress distributions in the core, the composite outer layer, and the composite insert were analyzed by FEM(finite element method), and then found optimal dimensions of the composite inserts.

2 Finite element model

2.1 Structural concept of a hybrid composite rotor

Fig.1 shows the cross-section view of a hybrid composite rotor for an ultracentrifuge. The rotor consists of the core, the composite inserts, and the composite outer layer. Almost all of the centrifugal forces are sustained by the composite outer layer, in which stiff carbon fibers are wound according to the circumferential direction. However, the weakest part is not the outer layer but the core or the composite inserts because of their relatively very low strength. If there is no composite insert, the circumferential stress are concentrated in the point *a* or *b* in Fig.1 where the radial thickness of the core has a minimum value, and the radial stress are concentrated in the point *c* in Fig.1 where the circumferential thickness of the core has a minimum value.

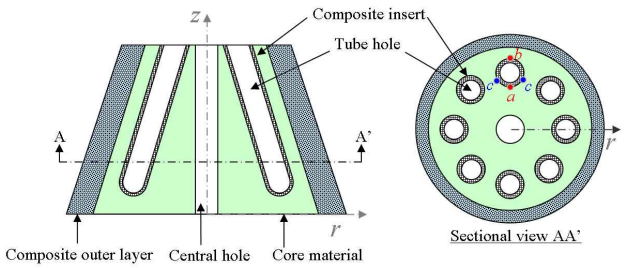

Fig.1. Cross-section view of a hybrid composite rotor for an ultracentrifuge.

2.2 Simplified slice disc model

When rotating, the rotor in Fig.1 experiences shear stress components σ_{zr} and $\sigma_{z\theta}$. Since the shear stresses transfer centrifugal loads from the bottom part of the rotor, which is in the higher stress level, to the top part of the rotor, which is in the lower

stress level, a stress analysis of a simplified slice disc based on the plane stress assumption gives conservative evaluation.

The dimensions of the model are as follows. As shown in the Fig.1, composite inserts are located not parallel to the z-axis, but with the inclined angle θ_{CI} from the z-axis. Thus, the cross-sectional shape of the composite insert on the r-θ plane is the ellipse whose minor radius is the same as the radius of the composite insert and whose major radius is one over $\cos\theta_{CI}$ times the radius of the composite insert. In this study, the inner radius of the composite insert was 5 mm. The two variables in this study, the thickness and the inclined angle θ_{CI} of the composite insert have the ranges from 1.6 mm to 2.2 mm and from 0° to 25°, respectively.

Fig.2 represents FE model to calculate stresses near the tube hole. Considering symmetric conditions, we constructed a 15° sliced disc model. The point A in Fig.2 is the position where the maximum G-force generated. The distance from the rotating axis to the point A is 40 mm. Since the rotating speed is 100,000 rpm, the G-force at A is 447,000 × g. The boundary radius between the core and the composite outer layer is 43 mm, and the inner radius of the core is 25.8 mm, i.e. 60% of the boundary radius. The outer radius of the composite outer layer is 51.3 mm, which is the optimal dimension of the composite outer layer suggested by the previous research[6]. The boundary conditions of the model are as follows. The inner and the outer radius are on the free boundary conditions, and the cutting out edges at θ of 0° and 15° are on the symmetric conditions. Its loading condition is applying centrifugal body forces only.

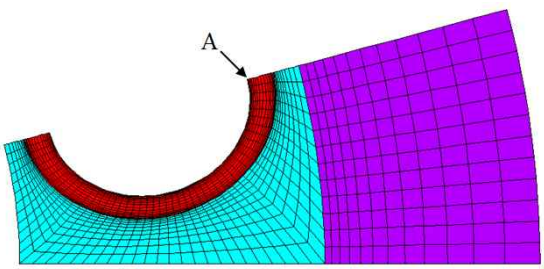

Fig.2. Finite element model to calculate stresses near the tube hole.

2.3 Material properties

Table 1 shows the material properties of the core, the composite insert, and the composite outer layer, which are PEI, Kevlar/epoxy composites, and AS4/3501-6, respectively. The material combination is the best one of the previous research that can generate the G-force with the lowest stress level[6].

Table 1 Material properties

			PEI	Kevlar/ epoxy	AS4/ 3501-6
Stiffness [GPa]		E_{11}	3.0	76.8	148
		E_{22}		5.5	10.5
Shear modulus [GPa]		G_{12}	-	2.07	5.61
		G_{23}		1.40	3.17
Poisson's ratio		ν_{12}	0.36	0.34	0.30
		ν_{23}		0.37	0.59
Density [kg/m^3]		ρ	1270	1380	1520
Strength [MPa]	Tensile	S_{11T}	105	1380	53.4
		S_{22T}		27.6	2137
	Compressive	S_{22C}	-	-	238
	Shear	S_{12}	-	49	89
Fiber volume fraction		V_f	-	0.55	0.62

2.4 Coordinate systems

As shown in Fig.3, two kinds of coordinate systems are used in this study, global cylindrical coordinates whose origin is on the rotating axis of the centrifuge and local elliptical coordinates whose origin is on the center of the ellipse. Material properties are assigned to the core and the composite outer layer according to the global cylindrical coordinates, and to the composite insert according to the local elliptical coordinates. Since the composite insert is inclined to the r-θ plane of the simplified model, its properties should be translated from the ply coordinates of the insert to the local elliptical coordinates of the model.

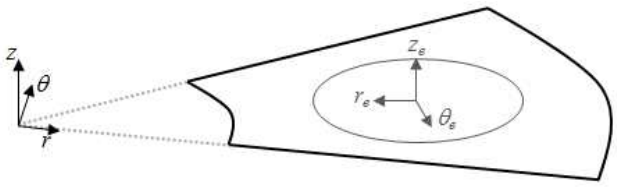

Fig.3. Coordinate systems used in the analysis; global cylindrical coordinates and local elliptical coordinates.

2.5 Analysis condition

To analyze the model, we used the commercial software *ANSYS 11*. Since this model should be able to deal with anisotropic materials (the composite insert) as well as orthotropic and isotropic materials (the composite outer layer and the core), we chose the PLANE 183 elements that can handle the plane stress problems of anisotropic materials.

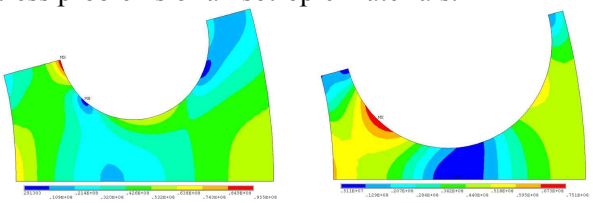

(a) (b)

Fig.4. Von Mises stress distribution of the core: (a) a hybrid rotor having no the composite insert, (b) a hybrid rotor having the composite inserts.

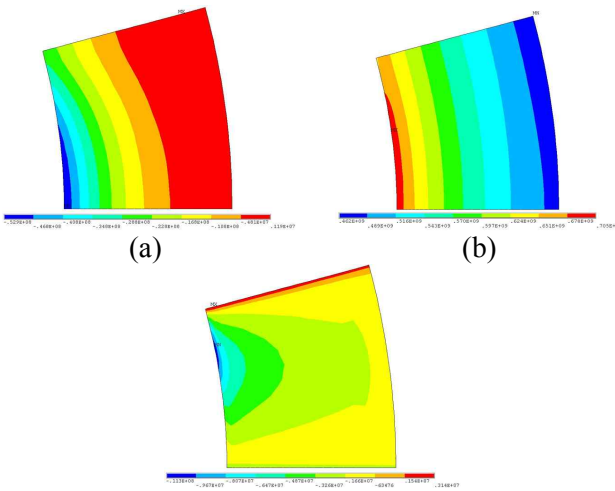

(a) (b) (c)

Fig.5. Stress distributions of the composite outer layer in the global cylindrical coordinates: (a) σ_{rr}, (b) $\sigma_{\theta\theta}$, (c) $\sigma_{r\theta}$.

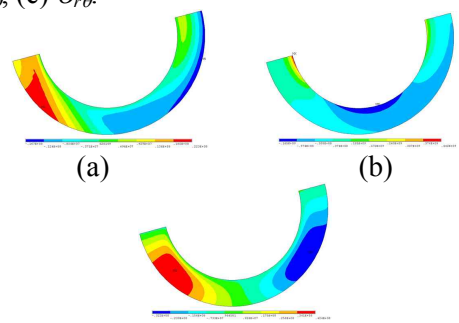

(a) (b) (c)

Fig.6. Stress distribution of the composite insert in the local elliptical coordinates: (a) σ_{rr}, (b) $\sigma_{\theta\theta}$, (c) $\sigma_{r\theta}$.

3 Result and discussion

3.1 Stress distributions

Fig.4 shows the effect of the composite insert on the stress concentration of the core material. When a hybrid rotor having 15° inclined tube holes but no composite insert rotates at 100,000 rpm, the maximum von Mises stress occurs at the inside of the tube hole where θ_e in the local elliptical coordinates is 0°, i.e. the red color in Fig.4(a). However, when a hybrid rotor having the composite inserts whose thickness is 1.9 mm rotates at the same speed, the maximum von Mises stress occurs at the inside of the tube hole where θ_e is about 30°, and the maximum stress value reduces by 21.4% from 95.5MPa to 75.1MPa.

Fig.5 represents stress distributions of the composite outer layer. The maximum of the compressive radial stresses is 52.9MPa, and the maximum of the tensile circumferential stress is 705MPa. The other stress components are negligible. Since those stresses are much smaller than the strengths of AS4/3501-6 in Table 1, the composite outer layer is not a critical component of the hybrid composite rotor.

Fig.6 is the stress distributions of the composite insert in the local elliptical coordinates. The maximum of the radial stress occurs at the same position where the maximum von Mises stress of the core occurs, and its value is 22.3MPa. The maximum of the circumferential stress occurs at the inside of the tube whole where θ_e in the local elliptical coordinates is 0°, and its value is 442MPa. The maximum of the shear stress is 42.4MPa. Since the ply coordinates of the composite insert is different from the local elliptical coordinates, the stresses should be transformed to the ply coordinates in order to compare them with the strengths of the insert. In the following two sections, stresses of the composite insert will be described in the ply coordinates.

3.2 Effect of the insert's inclined angle

Fig.7 shows the ratio of maximum stresses to the material strengths with respect to the inclined angle of the composite insert whose thickness is 1.9 mm. Four major stress components that have relatively large values compared to the strengths are shown in the graph. As the inclined angle increases, the shear

stress σ_{13} of the composite insert decreases, but the tensile stress σ_{33} and the shear stress σ_{12} of the composite insert soar. In the case of the core, the von Mises stress increases very slowly.
In Fig.7, the case that gives the best margin of safety is when the shear stresses σ_{12} and σ_{13} have the same value.

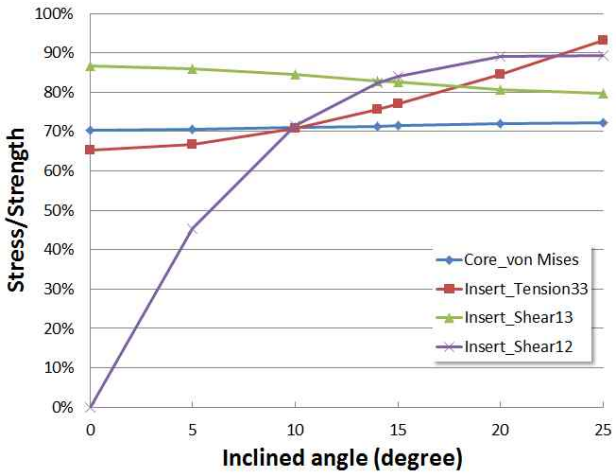

Fig.7. Ratio of maximum stresses to the material strengths with respect to the inclined angle of the composite insert whose thickness is 1.9 mm.

3.3 Effect of the insert's thickness

Figs.8 and 9 represent the effect of the insert's thickness. In Fig.8, the ratio of maximum stresses to the material strengths when $\sigma_{13} = \sigma_{12}$ decreases as the composite insert become thicker. However, the ratio when $\sigma_{13} = \sigma_{33}$ increases. Thus, we can find the cross point of the two lines, i.e. the optimal point having the largest margin of safety.
The similar trend occurs in Fig.9. As the thickness of the composite becomes thicker, the inclined angle when $\sigma_{13} = \sigma_{12}$ increases, but the inclined angle when $\sigma_{13} = \sigma_{33}$ decreases. Thus the two line meet each other, and the cross point is related to the optimal point in Fig.8.
From Figs.8 and 9, the optimal condition of the composite insert that can minimize the stress level in the simplified slice disc model is when the thickness and the inclined angle of the composite insert are 2.15 mm and 15.4°, respectively. At that condition with the rotating speed of 100,000 rpm, the shear stresses of the composite insert rises up to 82.3% of the shear strengths. That means the shear stresses equal the ultimate shear strengths when the rotating speed of the disc is 110,000 rpm. Hence, the maximum *G*-force of the model is 540,000 × g.
The calculation result based on the simplified slice disc model gives higher stress level than that of 3-D structure as shown in Fig.1. Therefore, we can expect that the hybrid composite rotor equipped with the composite inserts optimized in this study can sustain centrifugal forces up to the *G*-force of an ultracentrifuge level.

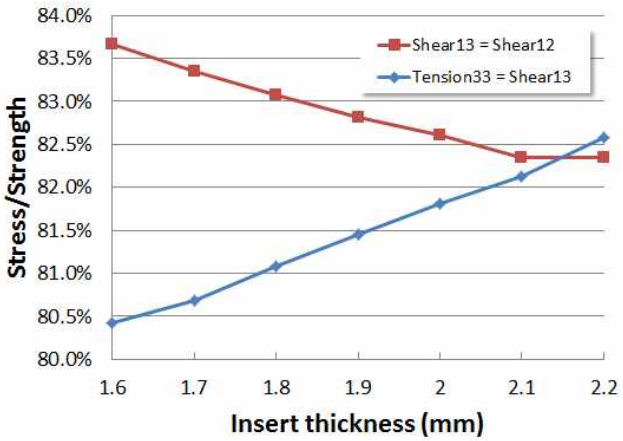

Fig.8. Ratio of maximum stresses to the material strengths when $\sigma_{33} = \sigma_{13}$ and when $\sigma_{13} = \sigma_{12}$.

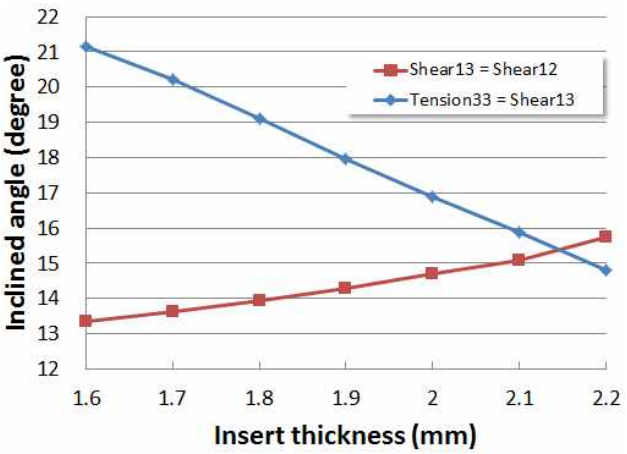

Fig.9. Inclined angle of the composite insert when $\sigma_{33} = \sigma_{13}$ and when $\sigma_{13} = \sigma_{12}$.

4 Conclusion

In this study, one of the components of the hybrid composite rotor, the composite insert was optimized by FE analysis using a simplified slice disc model.

The shear stress of the composite insert was the largest stress in the hybrid composite rotor structure, and was minimized when the thickness and the inclined angle of the composite insert are 2.15 mm and 15.4°, respectively, for the given dimensions of the rotor in this study. At this condition, we can raise the *G*-force of the model up to 540,000 × g. Since the 3-D structure of the hybrid composite rotor has lower stress level than the simplified model does, it can be concluded that the hybrid composite rotor equipped with the optimized composite insert is one of the plausible rotor structures for an ultracentrifuge.

Acknowledgement

This study was performed as a part of the project, "Development of the design theory of a composite hybrid rotor to achieve extreme *G*-force," supported by Korea Institute of Materials Science (KIMS) in 2011.

References

[1] S.P. Timoshenko and J.N. Goodier "*Theory of Elasticity*". McGraw-Hill, 1970.
[2] S. Tang "Elastic stresses in rotating anisotropic disks". *International Journal of Mechanical Sciences*, Vol. 11, pp 509-517, 1969.
[3] G. Belingardi, G. Genta, and M. Gola "A study of the stress distribution in rotating, orthotropic discs". *Composites*, Vol. 10, No. 2, pp 77-80, 1979.
[4] X. Hai-jun and S. Jian "Failure analysis and optimization design of a centrifuge rotor". *Engineering Failure Analysis*, Vol. 14, pp 101-109, 2007.
[5] C.R. Joe, S.C. Kim, and J.K. Park, "A study on the design of filament wound centrifuge rotor". *KSPE Autumn Conference*, pp 835-838, 1999.
[6] H.G. Lee, J. Park, B.S. Hwang, and J.H. Kim, "Design theory and optimization method of a hybrid composite rotor for an ultracentrifuge," *Composite Structures* (applied).